Single landmark distance-based navigation

Nguyen, Thien-Minh; Qiu, Zhirong; Cao, Muqing; Nguyen, Thien Hoang; Xie, Lihua

2019

Nguyen, T.-M., Qiu, Z., Cao, M., Nguyen, T. H., & Xie, L. (2019). Single landmark distance-based navigation. IEEE Transactions on Control Systems Technology, 28(5), 2021-2028. doi:10.1109/TCST.2019.2916089

https://hdl.handle.net/10356/144413

https://doi.org/10.1109/TCST.2019.2916089

Single Landmark Distance-Based Navigation

Thien-Minh Nguyen, Zhirong Qiu, Muqing Cao, Thien Hoang Nguyen, and Lihua Xie, *Fellow, IEEE*

***Abstract*— In this brief, we study the distance-based navigation problem of unmanned aerial vehicles (UAVs) by using a single landmark placed at an arbitrarily unknown position. To solve the problem, we propose an integrated estimation-control scheme to simultaneously accomplishes two objectives: relative localization using only distance and odometry measurements, and navigation to the desired location under bounded control input. Asymptotic convergence is obtained by invoking the discrete-time LaSalle's invariance principle in the noise-free case, and the stability under distance measurement noise is also investigated. We also validate our theoretical findings on quadcopters equipped with ultra-wideband ranging sensors and optical flow sensors in a global positioning system (GPS)-less environment.**

***Index Terms*— Adaptive control, discrete-time, docking, GPS-denied, input saturation, micro aerial vehicles, ranging, relative localization.**

I. Introduction

RECENT decade has witnessed a dramatic surge in popularity of small-scaled unmanned aerial vehicles (UAVs) with applications in many areas, e.g., aerial photography, logistical delivery, and surveillance. Essentially, the successful maneuver of UAVs, or mobile robots in general, needs to solve two problems: localization and navigation, or estimation and control in a more general sense. These two problems are usually addressed in a separate manner for a convenient solution and analysis. Most commonly, we find that localization capability is the primal assumption, based on which different navigation tasks can be fulfilled.

Generally, there exist two methods to achieve accurate and reliable localization. The first method relies on some kind of localization infrastructure, such as global positioning system (GPS), ultra-wideband (UWB) localization system [2]–[5], or indoor positioning systems based on routers [6]. This is undoubtedly the most viable way to realize many large-scale control schemes in the literature such as flocking [7], [8], formation [9]–[11], or interception [12]. However, the requirement of infrastructure in these systems not only results in limited coverage but also incurs additional deployment and maintenance costs, including labor-intensive calibration and troubleshooting. Consequently, applications based on these system have low adaptability to different and complex environments. On the other hand, recent advances in vision-based localization techniques have offered a much more flexible method for UAV localization [13], [14], by only using onboard sensors. Although no infrastructure is needed in this case, the key issue with vison-based localization techniques is that they are only accurate in estimating the short-term displacement while long-term operations would lead to drift in positioning estimation. Based on the above-mentioned consideration, new methods need to be proposed to allow operation of UAVs with minimal deployment cost and adequate flexibility.

In this work, we first study the single landmark docking problem by combining odometry and distance measurements to the landmark at an unknown position, when no external localization system is available. In this navigation task, the UAV is required to dock at the stationary landmark without absolute positioning information. An integrated localization–navigation scheme is proposed to solve this problem: we employ an adaptive estimation scheme to estimate the relative position to the landmark, and also delicately design a control scheme to ensure asymptotic convergence of the estimation as well as the docking objectives. Motivated for practical implementation, we also consider a discrete-time formulation and control input saturation. By employing adaptive control techniques and the discrete-time LaSalle's invariance principle, the efficacy of the overall localization–navigation scheme is rigorously established. We also discuss the stability under distance measurement error, as well as extending the docking scheme to arbitrary locations relative to the landmark. Experiments are conducted on quadcopters to validate the result.

Some related works can be found in [15]–[21] with similar premise, focusing on two types of navigation problems: a circumnavigation problem where an UAV is required to circle around a stationary or moving target [15]–[19], and a target pursuit or docking problem where an UAV is required to navigate to the prescribed position relative to the fixed landmark(s) [20], [21]. Different techniques have been proposed to solve these two problems. Specifically, for UAVs modeled by unicycle dynamics, the distance measurements and the corresponding change rate were employed to tune the heading of the UAV toward the landmark [15]–[18]. On the other hand, based on adaptive estimation techniques [22], [25], certain kinds of trajectories were designed to simultaneously fulfill the localization and navigation tasks [19]–[21]. In comparison with the above works for continuous-time dynamics, our work considers a discrete-time formulation, which saves

Manuscript received January 23, 2019; accepted April 26, 2019. Manuscript received in final form May 4, 2019. This work was supported in part by the ST Engineering - NTU Corporate Laboratory under the National Research Foundation (NRF) Singapore Corporate Laboratory@University Scheme. Recommended by Associate Editor T. Shima. This paper was partially presented at 2018 IEEE/RSJ International Conference on Intelligent Robots and Systems, Madrid, Spain, October 2018 [1]. *(Corresponding author: Zhirong Qiu.)*

The authors are with the School of Electrical and Electronic Engineering, Nanyang Technological University, Singapore 639798 (e-mail: e150040@e.ntu.edu.sg; qiuz0005@e.ntu.edu.sg; caom0006@e.ntu.edu.sg; e180071@e.ntu.edu.sg; elhxie@ntu.edu.sg).

This paper has supplementary downloadable material available at http://ieeexplore.ieee.org, provided by the author.

Color versions of one or more of the figures in this paper are available online at http://ieeexplore.ieee.org.

Digital Object Identifier 10.1109/TCST.2019.2916089

the trouble of gain tuning and is hence more convenient for implementation. The most important difference from the relevant works [20], [21] is that we only use distance and odometry measurements without requiring the absolute position information. This allows the algorithm to be readily compatible with operation in GPS-denied environments, where accurate short-term displacement measurement obtained from visual odometry (VO) is usually the most suitable alternative. In addition, we also consider the issue of control input saturation, which was not addressed in the above two works. Finally, we implement the proposed scheme on quadcopters and conduct experiments to validate the theoretical findings and applicability of the proposed scheme.

The remainder of this brief is organized as follows. After introducing the problem formulation along with the dynamics and sensor models in Section II, we proceed to propose the distance-based relative localization and control laws in Section III. We then provide the analyses on stability and convergence of the docking task in Section IV. We then put forth some discussions on more practical scenarios with relative docking as well as influence of noise in Section V. Simulation and experiment results are, respectively, provided in Sections VI and VII to validate the theory and demonstrate the practicality of the proposed algorithm. Section VIII concludes our work.

Notations: we, respectively, use $\mathbf{N}$, $\mathbf{R}$, and $\mathbf{R}^+$ to denote the set of natural numbers, the set of real numbers, and the set of positive real numbers. For a vector $v \in \mathbf{R}^m$, $\|v\|$ and $\|v\|_\infty$, respectively, stand for the Euclidean norm and the infinity norm, and v' denotes its transpose. For a set $G \subset \mathbf{R}^m$, $\bar{G}$ denotes the closure of G. $\bar{\mathcal{B}}(p, r)$ denotes the open ball centered at p with radius r.

II. Problem Statement

Given a landmark arbitrarily deployed at an unknown position p^*, the docking problem is solved if we can design a control law to achieve the following objective:

$$\lim_{k\to\infty} p_k = p^* \tag{1}$$

where p_k is the UAV's position in the same frame of reference of p^*. The UAV is modeled as a discrete-time integrator with bounded velocity as follows:

$$p_{k+1} = p_k + T\bar{u}_k, \quad \|\bar{u}_k\|_\infty \le U \tag{2}$$

where T is the sampling period and U is the maximum velocity. Clearly, for any control input u_k, the bounded velocity requirement can be satisfied by letting $\bar{u}_k = \pi_U(u_k)$ where $\pi_U(\cdot)$ is a projection operator onto $\bar{\mathcal{B}}(0, U) \subseteq \mathbf{R}^m$ defined by

$$\pi_U(u_k) \triangleq s_U(u_k)u_k, \quad s_U(u_k) \triangleq U/\max\{U, \|u_k\|\}. \tag{3}$$

In the sequel, we also write $s_k = s_U(u_k)$ for conciseness.

In navigation, the UAV can obtain two types of measurements: distance measurement d_k and displacement ϕ_k, whose definitions and some mathematical relationships with other quantities are stated as follows:

$$d_k \triangleq \|q_k\| = \|p_k - p^*\| \tag{4}$$

$$\phi_k \triangleq p_{k+1} - p_k = q_{k+1} - q_k = T\bar{u}_k \tag{5}$$

where $q_k \triangleq p_k - p^*$ is the position of the UAV relative to the landmark and $\phi_k = T\bar{u}_k$ is a result of the dynamics (2).

Remark 1: It should be pointed out that the displacement ϕ_k is obtained from onboard sensors, rather than from differentiating two consecutive absolute positions. Specifically, with the mature development of VO or simultaneous localization and mapping (SLAM) techniques, it can be obtained accurately by calculating the displacement of visual features in two consecutive camera image frames. In the experiment later, we obtain ϕ_k from a generic commercial optical flow sensor, which operates in the same principle with VO techniques.

III. Integrated Localization–Navigation Scheme

In this section, we shall design an integrated localization and navigation scheme to simultaneously solve the relative localization and docking problem. To be detailed, an adaptive estimator based on distance and odometry measurements is designed to achieve the relative localization, then based on which $\bar{u}_k$ is designed in a particular form to solve the docking problem (1). See Sections III-A and III-B for details.

A. Adaptive Estimator for Relative Localization

From (4) and (5), we get the following equality:

$$\begin{aligned} d_k^2 - d_{k-1}^2 &= \|q_{k-1} + \phi_{k-1}\|^2 - \|q_{k-1}\|^2 \\ &= \|\phi_{k-1}\|^2 + 2\phi_{k-1}' q_{k-1}. \end{aligned}$$

Now, we can define the following parametric model:

$$\zeta_k = \frac{1}{2}\left(d_k^2 - d_{k-1}^2 - \|\phi_{k-1}\|^2\right) = \phi_{k-1}' q_{k-1}. \tag{6}$$

Let us denote $\hat{q}_k$ as the estimate of the relative position q_k and $\epsilon_k = \zeta_k - \phi_{k-1}'\hat{q}_{k-1}$ as an observation innovation. The following law is used for updating the relative position estimate $\hat{q}_k$ when new measurements are obtained:

$$\hat{q}_k = \pi_{d_k}(\hat{q}_{k-1} + \phi_{k-1} + \gamma\,\phi_{k-1}\epsilon_k), \quad \gamma > 0. \tag{7}$$

Remark 2: In [23] and [24] a similar parametric model was used to construct an adaptive estimator for the relative localization objective. However, in these works additional observers were required to estimate the derivative of distance measurements, which is not the case for the discrete-time model in our work. Furthermore, both of the above works only considered the cooperative relative localization for multi-agents, and the navigation problem was not discussed.

B. Bounded Control Law for Navigation

Based on the estimator (7), the following bounded controller is proposed to solve the docking problem (1):

$$\bar{u}_k = \pi_U(u_k), \quad u_k = -\beta\hat{q}_k + \alpha d_k \sigma_k, \ \alpha, \beta > 0 \tag{8}$$

where $\sigma_k \in \mathbf{R}^m$ is an internal signal generated by an autonomous system

$$\rho_{k+1} = \Pi(\rho_k), \quad \sigma_k = \Sigma(\rho_k), \ k = 0, 1, 2, \ldots \tag{9}$$

where Π and Σ are two continuous mappings chosen to satisfy the following assumptions.

Assumption 3:

1) $\Pi\colon \mathcal{S} \to \mathcal{S}$ with $\mathcal{S} \subseteq \mathbf{R}^n$ being compact.
2) $\bar{\sigma} = \sup\{\|\sigma_k\|, k = 0, 1, \dots\} \leq 1$.
3) There exists $K \in \mathbf{N}$ such that $\sigma_{k+K} = -\sigma_k, \forall k \in \mathbf{N}$; moreover, $\text{span}\{\sigma_k\colon k = 0, 1, \dots, K-1\} = \mathbf{R}^m$.

In the following, we consider the case of $m = 2$ and $m = 3$, respectively, corresponding to the cases of 2-D and 3-D localizations. In both cases, we take $\mathcal{S} = \{\rho = [\rho_1, \rho_2]' \in \mathbf{R}^2\colon \|\rho\| = 1\}$, and define Π to be a matrix operator as

$$\Pi = \begin{bmatrix} \cos\omega & -\sin\omega \\ \sin\omega & \cos\omega \end{bmatrix} \tag{10}$$

where $\omega = 2\pi/N$ and N is an even integer. Based on this, we generate the signal σ_k by defining Σ as follows:

$$\Sigma(\rho) = \begin{cases} \rho, & m = 2 \\ \big[r_1\rho_1,\ r_1\rho_2,\ r_2\big(4\rho_1^3 - 3\rho_1\big)\big]', & m = 3 \end{cases} \tag{11}$$

where r_1 and r_2 are two positive constants satisfying $r_1^2 + r_2^2 = 1$. Note that N is to be selected as in the following lemma.

Lemma 4: The mappings Π, Σ defined by (10) and (11) will satisfy Assumption 3 for all $\rho_0 \in \mathcal{S}$ if $N \geq 4$ for $\mathbf{R}^2$ and $N \geq 8$ for $\mathbf{R}^3$.

Proof: Given $\rho_0 = [\cos\varphi \ \ \sin\varphi]' \in \mathcal{S}$ for some $\varphi \in [0, 2\pi]$ and using the definitions (10) and (11), we can obtain $\sigma_k = [\cos(k\omega + \varphi),\ \sin(k\omega + \varphi)]'$ in $\mathbf{R}^2$. The result can be established by noting that $\det[\sigma_k\ \sigma_{k+1}] = \sin(2\pi/N) \neq 0$ for an even integer $N \geq 4$ in the 2-D case. Similarly, in $\mathbf{R}^3$, we can verify that $\sigma_k = [r_1\cos(k\omega+\varphi),\ r_1\sin(k\omega+\varphi),\ r_2\cos(3k\omega+3\varphi)]'$ and $\det S = \det[\sigma_k\ \sigma_{k+1}\ \sigma_{k+2}] = \mathcal{A}\cos(\mathcal{B}k + \mathcal{C})$, where $\mathcal{A} \triangleq r_1^2 r_2\big[\sin(8\pi/N) - 2\sin(4\pi/N)\big]$, $\mathcal{B} \triangleq 6\pi/N$, and $\mathcal{C} \triangleq 3\varphi + 6\pi/N$. By noticing $\mathcal{A}$, we can establish that for $N \geq 8$, there is at least a step $k^* \in \{0, 1, N-1\}$ that $\det S \neq 0$ for the 3-D case. ∎

Remark 5: Note that a function $f(d_k)$ satisfying $f(0) = 0$, $0 < f(d) \leq d$, $\forall d > 0$ can be used in place of d_k in the control law (8) without affecting any result on stability and convergence. We have conducted simulations as well as experiments with $f(d_k) = 10(1 - e^{-10d_k})$ and found that the convergence is slower than the case of $f(d_k) = d_k$, hence the choice of $f(d) = d$ in the current control law.

IV. Convergence Analysis

In this section, we will first establish the stability of the system state, and then invoke LaSalle's Invariance Principle to achieve the docking objective (1).

A. Stability Analysis

Denote $\tilde{q}_k = \hat{q}_k - q_k$ as the estimation error for relative localization, and note that $q_k = p_k - p^*$ is the position error for navigation. In this section, we shall show the boundedness of $\tilde{q}_k$ and q_k, respectively, in Propositions 6 and 7 below. Specifically, we consider the following condition:

$$\gamma\,(TU)^2 < 2, \quad \alpha < \beta < 1/T \tag{12}$$

where γ, β, and α are constants. Note that for fixed γ and α, both of the above conditions can be met by a small sampling period T. On the other hand, for a fixed T, they can be satisfied by small γ and α. The following two propositions, respectively, establish the boundedness for the estimation error and the position error.

Proposition 6 (Boundedness of Estimation Error): Under the estimator (7) and the condition $\gamma\,(TU)^2 < 2$, it holds that $\|\tilde{q}_k\| \leq \|\tilde{q}_0\|$ and $\epsilon_k \in \ell_\infty \cap \ell_2$.

Proof (Sketch): By defining $\bar{q}_k \triangleq \hat{q}_{k-1} + \phi_{k-1} + \gamma\,\phi_{k-1}\epsilon_k$ and $g_k \triangleq \pi_{d_k}(\bar{q}_k) - \bar{q}_k$, we obtain the dynamics of $\tilde{q}_k$ as follows:

$$\tilde{q}_k = \bar{q}_k + g_k - q_k = \big(I - \gamma\,\phi_{k-1}\phi_{k-1}'\big)\tilde{q}_{k-1} + g_k. \tag{13}$$

From the error dynamics (13), we can define a Lyapunov-like function $V_k \triangleq \gamma^{-1}\tilde{q}_k'\tilde{q}_k$ and examine its rate of change $\Delta V_{k+1} = V_{k+1} - V_k$ using similar procedures that were used to prove [26, Lemma 4.1.1 and Th. 4.10.4]. From this examination and the assumption $\gamma\,(TU)^2 < 2$, we can see that $\forall k \geq 0$, $\Delta V_{k+1} \leq -\epsilon_{k+1}^2(2 - \gamma\,\phi_k'\phi_k) \leq 0$. Hence $\tilde{q}_k \in \ell_\infty$ and $\epsilon_k \in \ell_\infty \cap \ell_2$. ∎

Proposition 7 (Ultimate Boundedness of Docking Error): Under the estimator (7) and the bounded controller (8), let condition (12) and Assumption 3 hold. Given the initial relative estimation error $\tilde{q}_0$ and position error q_0, there exists a constant $M(\tilde{q}_0)$ to satisfy the following statements.

1) If $q_{k_0} \in \mathcal{M} \triangleq \bar{\mathcal{B}}(0, M(\tilde{q}_0))$ for some k_0, then $q_k \in \mathcal{M}$ for $k \geq k_0$.
2) There exists a time step $k_0(q_0, M)$ such that $q_{k_0} \in \mathcal{M}$.

Consequently, $\limsup_{k\to\infty}\|q_k\| \leq M(\tilde{q}_0)$ for any q_0.

Proof: Define $D_k = d_k^2$ and $\Delta D_k = D_k - D_{k-1}$. Recalling the definition of π_U in (3), we obtain by (5) that

$$\begin{aligned} \Delta D_k &= (q_k + T\bar{u}_k)'(q_k + T\bar{u}_k) - q_k'q_k \\ &= s_k T\big(s_k T u_k'u_k + 2u_k'q_k\big), \quad s_k \triangleq s_U(u_k) \end{aligned} \tag{14}$$

which gives rise to $\Delta D_k/(s_k T) \leq Tu_k'u_k + 2u_k'q_k \triangleq \Delta\tilde{D}_k$ as a result of $s_k \in (0, 1]$. By substituting $u_k = -\beta(q_k + \tilde{q}_k) + \alpha\|q_k\|\sigma_k$ into $\Delta\tilde{D}_k$ as $\|q_k\| = d_k$, we get that (the subscript $(\cdot)_k$ shall be omitted to keep the notation concise)

$$\begin{aligned} \Delta\tilde{D} &= T\beta^2(\|q\|^2 + \|\tilde{q}\|^2 + 2\tilde{q}'q) + T\alpha^2\|q\|^2\|\sigma\|^2 \\ &\quad - 2T\beta\alpha\|q\|\sigma'(q+\tilde{q}) - 2\beta(\|q\|^2 + \tilde{q}'q) + 2\alpha\|q\|\sigma'q \\ &= (T\beta^2 - 2\beta)\|q\|^2 + T\alpha^2\|q\|^2\|\sigma\|^2 \\ &\quad + (2 - 2T\beta)\alpha\|q\|\sigma'q + (2T\beta^2 - 2\beta)\tilde{q}'q \\ &\quad - 2T\beta\alpha\|q\|\sigma'\tilde{q} + T\beta^2\|\tilde{q}\|^2 \\ &\leq [T\beta^2 + T\alpha^2 - 2\beta + (2 - 2T\beta)\alpha]\|q\|^2 \\ &\quad + 2\beta[(1 - T\beta) + T\alpha]\|q\|\|\tilde{q}\| + T\beta^2\|\tilde{q}\|^2 \end{aligned} \tag{15}$$

where to attain the last inequality we have used the condition $\|\sigma_k\| \leq 1$ in Assumption 3, $1 - T\beta > 0$, as well as Cauchy–Schwartz inequality. Furthermore, by recalling (12), it is readily seen that the coefficient of $\|q_k\|^2$ is given by

$$\begin{aligned} T\beta^2 + T\alpha^2 - 2\beta + (2 - 2T\beta)\alpha &= (\beta - \alpha)[T(\beta - \alpha) - 2] \\ &\leq -(\beta - \alpha)(T\alpha + 1) < 0. \end{aligned}$$

Thus, in combination with $\|\tilde{q}_k\| \leq \tilde{Q} \triangleq \|\tilde{q}_0\|$ in Proposition 7, we have

$$\Delta D_k \leq s_k T\big(-a\|q_k\|^2 + b\|q\| + c\big) \tag{16}$$

where $a = (\beta - \alpha)(T\alpha + 1)$, $b = 2\beta[(1 - T\beta) + T\alpha]\tilde{Q}$, and $c = T\beta^2\tilde{Q}^2$. Therefore, $\Delta D_k < 0$ for $q_k > \tilde{M}(\tilde{q}_0) \triangleq (b + (b^2 + 4ac)^{1/2})/(2a)$.

Consequently, if we take $M = \tilde{M}(\tilde{q}_0) + TU$, then the statement 1 can be achieved by the following induction: if $\|q_{k_0}\| \leq \tilde{M}$, then $\|q_{k_0+1}\| \leq M$ by noticing the bounded input (2); if $\tilde{M} < \|q_{k_0}\| \leq M$, then $\|q_{k_0+1}\| < \|q_{k_0}\| \leq M$.

On the other hand, if $\|q_0\| \leq M$ then the statement 2 is finished. Otherwise, we know that $\|q_k\| \leq \|q_0\|$ for all k, and $\|u_k\| \leq \beta\tilde{Q} + \alpha\|q_0\|$. Hence, $s_k = U/\max\{U, \|u_k\|\} \geq U/\max\{U, \beta\tilde{Q} + \alpha\|q_0\|\} > 0$. Moreover, it can be seen that $-a\|q_k\|^2 + b\|q\| + c \leq -aM^2 + bM + c < 0$ for $\|q_k\| \geq M$; in this case, we can obtain from (16) that

$$\Delta D_k \leq TU/\max\{U, \beta\tilde{Q} + \alpha\|q_0\|\}(-aM^2 + bM + c) \quad (17)$$

implying that $\|q_k\|$ will keep decreasing until $q_{k_0} \in \mathcal{M}$ for some time step k_0, which is the statement 2. ■

B. Convergence

Now, we are ready to assert the convergence of q_k to 0 by invoking the LaSalle's invariance principle for discrete-time autonomous systems [27] as follows.

Theorem 8: Under Assumption 3, the distance-based docking problem (1) can be solved by combining the adaptive estimator (7) and the bounded controller (8), if we select proper gains to satisfy conditions (12).

Proof: The overall system is given by combining the update protocol of q_k, $\tilde{q}_k$,and ρ_k, respectively, in (5), (13), and (9) as follows:

$$\begin{aligned} q_{k+1} &= q_k + \phi_k \\ \tilde{q}_{k+1} &= \pi_{d_{k+1}}\big[q_k + \phi_k + \big(I - \gamma\phi_k\phi_k'\big)\tilde{q}_k\big] - (q_k + \phi_k) \\ \rho_{k+1} &= \Pi(\rho_k), \quad k = 0, 1, 2, \ldots \end{aligned} \quad (18)$$

where $\phi_k = T\bar{u}_k = Ts_k u_k$, $u_k = -\beta(q_k + \tilde{q}_k) + \alpha\|q_k\|\sigma_k$, and $\sigma_k = \Sigma(\rho_k)$. Clearly, (18) defines a continuous map on $\mathbf{R}^m \times \mathbf{R}^m \times \mathcal{S}$, where $\mathcal{S}$ is defined in Assumption 3. In addition, by Propositions 6 and 7, for any given initial relative position error q_0 and estimation error $\tilde{q}_0$, there exists a time step k_0 such that $[q_k', \tilde{q}_k', \rho_k']' \in \mathcal{G} \triangleq \tilde{\mathcal{Q}} \times \mathcal{M} \times \mathcal{S}$ for $k \geq k_0$, where $\tilde{\mathcal{Q}} = \bar{\mathcal{B}}(0, \|\tilde{q}_0\|)$ and $\mathcal{M}$ is defined in Proposition 7. Therefore, without loss of generality, we only need to consider the trajectory starting within $\mathcal{G}$, and it can be concluded from Propositions 6 and 7, and Assumption 3 that $\mathcal{G}$ is positively invariant under (18). Moreover, $\mathcal{G}$ is a compact set by recalling Propositions 6 and 7, as well as condition 1 of Assumption 3, and hence LaSalle's invariance principle [27] can be applied.

By LaSalle's Invariance Principle, all trajectories in $\mathcal{G}$ will converge to the maximum invariant set $\bar{\mathcal{I}} \subseteq \mathcal{G}$ satisfying $\Delta V_k \equiv 0, \forall k \in \mathbf{N}^+$, where V is the Lyapunov function defined in the proof of Proposition 6. We shall show that for any trajectory $\{[q_k', \tilde{q}_k', \rho_k']'\}_{k=0}^{\infty} \in \bar{\mathcal{I}}$, it must hold that $q_k \equiv 0$. Note that in the sequel, we abuse the notation of q_k, $\tilde{q}_k$, and ρ_k to denote the trajectory in $\bar{\mathcal{I}}$.

In fact, it is readily seen from the proof of Proposition 6 that $\Delta V_k \equiv 0$ iff $\epsilon_k = -\phi_{k-1}'\tilde{q}_{k-1} \equiv 0$, which, due to (13), also implies that $\tilde{q}_k \equiv \tilde{q}_0$. Below, we consider $\phi_k'\tilde{q}_0 \equiv 0$ for 3 cases to establish that $\phi_k'\tilde{q}_0 \equiv 0$ dictates either $\phi_k \equiv 0$ or $\tilde{q}_0 = 0$.

Case 1: $\tilde{q}_0 \neq 0$ and $\phi_k \not\equiv 0$. In this case, we have two deductions as follows.

First, since $0 \equiv \phi_k'\tilde{q}_0 = (q_{k+1} - q_k)'\tilde{q}_0 = (\hat{q}_{k+1} - \hat{q}_k)'\tilde{q}_0$, we get that $\hat{q}_k'\tilde{q}_0 \equiv \hat{q}_0'\tilde{q}_0$.

Second, if $d_k = 0$, then $u_k = -\beta\tilde{q}_k = -\beta\tilde{q}_0$ and $\phi_k = -T\beta s_k\tilde{q}_0$, which follows that $\phi_k'\tilde{q}_0 = -\beta T s_k\|\tilde{q}_0\|^2 \neq 0$, a contradiction. Therefore, $d_k > 0, \forall k \in \mathbf{N}$.

On the other hand, $0 \equiv \phi_k'\tilde{q}_0$ also implies that $0 \equiv u_k'\tilde{q}_0 = [-\beta\hat{q}_k + \alpha d_k\sigma_k]'\tilde{q}_0$ or equivalently $\beta\hat{q}_0'\tilde{q}_0 \equiv \beta\hat{q}_k'\tilde{q}_0 = \alpha d_k\sigma_k'\tilde{q}_0$. Specifically, we have $d_k\sigma_k'\tilde{q}_0 = d_{k+K}\sigma_{k+K}'\tilde{q}_0$. If we remember $\sigma_{k+K} = -\sigma_k$ in Assumption 3, we can further obtain that

$$[d_k + d_{k+K}]\sigma_k'\tilde{q}_0 \equiv 0, \quad k = 0, 1, \ldots, K-1. \quad (19)$$

As a consequence of $d_k > 0$ for any k, the above can be simplified as $\sigma_k'\tilde{q}_0 \equiv 0$. In addition, note that $\text{span}\{\sigma_k : k = 0, 1, \ldots, K-1\} = \mathbf{R}^m$ in Assumption 3, we can find a linear combination of $\tilde{q}_0$ as $\tilde{q}_0 = \sum_{k=0}^{K-1} a_k\sigma_k$, which follows by (19) that $\|\tilde{q}_0\|^2 = \tilde{q}_0'\sum_{k=0}^{K-1} a_k\sigma_k = 0$, another contradiction.

In summary, $\phi_k'\tilde{q}_0 \equiv 0$ dictates that $\phi_k \equiv 0$ or $\tilde{q}_0 = 0$.

Case 2: $\phi_k \equiv 0$. In this case, $u_k \equiv 0$ and $q_k \equiv q_0$, which yields that $d_k \equiv d_0$ and $\hat{q}_k \equiv \hat{q}_0$. Since $u_k = -\beta\hat{q}_k + \alpha\|q_k\|d_k)\sigma_k \equiv 0$, we have $\alpha d_0\sigma_k \equiv \beta\hat{q}_0$. By remembering that $\text{span}\{\sigma_k : k = 0, 1, \ldots, K-1\} = \mathbf{R}^m$ in Assumption 3, the only possible case is that $d_0 = 0$, namely, $q_k \equiv 0$.

Case 3: $\tilde{q}_0 = 0$. In this case, the estimation error is always 0, and the relative position dynamics is simplified to

$$q_{k+1} = q_k + Ts_k(-\beta q_k + \alpha d_k\sigma_k) \quad (20)$$

where s_k was defined in (3). It is clear that $q^* = 0$ is a globally asymptotically stable equilibrium for (20) by noting from (15) that $\Delta\tilde{D}_k \leq -(\beta - \alpha)(T\alpha + 1)\|q_k\|^2$ if $\tilde{q}_0 = 0$.

In summary, we have completed the proof. ■

V. Further Discussion

In this section, we put forth some discussions regarding the practical implementation subject to noise as well as a wider application of the algorithm.

A. Stability Under Distance Measurement Error

In this section, we consider the stability in the presence of bounded distance measurement error. Denote $\hat{d}_k = d_k + e_k$ as the distance measurement at time step k, where e_k denotes the measurement error and $\|e_k\| \leq \bar{e}$.

Moreover, denote $\hat{\zeta}_k = (1/2)(\hat{d}_k^2 - \hat{d}_{k-1}^2 - \|\phi_{k-1}\|^2)$ and $\hat{\epsilon}_k = \hat{\zeta}_k - \phi_{k-1}'\hat{q}_{k-1}$. The corresponding relative position estimator is obtained by replacing ζ_k with $\hat{\zeta}_k$ in (7) as follows:

$$\hat{q}_k = \begin{cases} \hat{q}_{k-1} + \phi_{k-1} + \gamma\phi_{k-1}\hat{\epsilon}_k, & k \neq 2nK \\ \pi_{\hat{d}_k}(\hat{q}_{k-1} + \phi_{k-1} + \gamma\phi_{k-1}\hat{\epsilon}_k), & k = 2nK \end{cases} \quad (21)$$

where $n \in \mathbf{N}$. Note that the projection $\pi_{d_k}(\cdot)$ in (7) is help to increase the convergence speed of $\tilde{q}_k$, and its use is optional (the results in all previous propositions and theorems will still hold without this operation). In this section, it is only

performed every $2K$ steps by the rule (21) for the ease of analysis. Straightforwardly, because of noisy distance measurement, the bounded controller will become

$$\bar{u}_k = \pi_U(u_k), \quad u_k = -\beta\hat{q}_k + \alpha\hat{d}_k\sigma_k \tag{22}$$

We present the stability result in the following Theorem.

Theorem 9: Assume that $\mu \triangleq \alpha/\beta < 1$ and let $\beta = \nu\gamma$, $\alpha = \mu\nu\gamma$ with $\nu < c_0/(2T)$, where c_0 is a constant depending on T, U and $\{\sigma_k\}_{k=0}^{K-1}$. Under the adaptive estimator (21) and the bounded controller (22), as well as Assumption 3, the relative position error q_k satisfies $\|q_k\| \le 4U/\alpha$ for all k, provided that γ is sufficiently small and the distance measurement error is bounded by

$$\bar{e} < \frac{\mu(1-\mu)\nu}{13(\mu+1)KU}. \tag{23}$$

Remark 10: The above result implies that the system stability can be retained if the distance measurement error is small. Note that the choice of γ may be dependent on the initial position error, and the upper bound $4U/\alpha$ is conservative. More investigation is needed in the future to improve the result.

Proof: To show the stability, below we will first obtain the error dynamics, and then show the excitation of displacement ϕ_t over $[k, k+2K-1]$ for large d_k, and finally show the boundedness by a proper Lyapunov function.

1) Error Dynamics: Without loss of generality, we assume $k = 2nK$, and hence $\|\tilde{q}_k\| \le 2(d_k + \bar{e})$. Similar to the analysis in the error-free case, the estimation error of the relative position will evolve as follows:

$$\tilde{q}_{t+1} = (I - \gamma\,\phi_t\phi_t')\tilde{q}_t + \gamma\,\phi_t\tilde{\zeta}_{t+1} \tag{24}$$

where $t = k + j$ with $0 \le j < 2K-1$, $\tilde{\zeta}_{t+1} = d_{t+1}e_{t+1} - d_te_t + (1/2)(e_{t+1}^2 - e_t^2)$, and $\|\tilde{\zeta}_{t+1}\| \le \bar{e}^2 + \bar{e}(d_{t+1}+d_t) \le \bar{e}^2 + \bar{e}(2d_t + TU)$. For $j = 2K-1$, at step $k+j+1$, the projection operation will be activated, and by replacing $V = \|\tilde{q}\|^2$ in the proof of Proposition 6, we can show that

$$\|\tilde{q}_{k+j+1}\| \le \|(I - \gamma\,\phi_{k+j}\phi_{k+j}')\tilde{q}_{k+j} + \gamma\,\phi_{k+j}\tilde{\zeta}_{k+j+1}\|. \tag{25}$$

On the other hand, the relative position error will evolve as

$$q_{t+1} = (1 - T\beta s_t)q_t - T\beta s_t\tilde{q}_t + T\alpha s_t(d_t + e_t)\sigma_t \tag{26}$$

where $t = k + j$ and s_t was introduced in (3).

2) We first show that when d_k is sufficiently large, then ϕ_t is excited over $[k, k+2K-1]$, i.e., there exists $c_0 > 0$ such that $\sum_{j=0}^{2K-1}\phi_{k+j}\phi_{k+j}' \ge c_0\ I$. For simplicity, we assume $m = 2$, and $n_1, n_2 \in \{\sigma_k\}_{k=0}^{K-1}$ with $n_1 = [1,0]', n_2 = [0,1]'$. Since $\phi_t = T\pi_U(u_t) = T\beta\pi_{U/\beta}(\tilde{u}_t)$ with $\tilde{u}_t = -\hat{q}_t + \mu\hat{d}_t\sigma_t$, in the following, we will examine $\hat{q}_t$ and $\hat{d}_t$ for $t \in [k, k+2K-1]$. Intuitively, the excitation follows from the observation that the change of $\hat{d}_t\sigma_t$ would dominate that of $\hat{q}_t$ for large d_t.

For $j \in [0, 2K]$, it can be inferred from (24), (25) and $\|q_{k+j} - q_k\| \le 2KTU$ that

$$\|\hat{q}_{k+j} - \hat{q}_k\| \le \|\tilde{q}_{k+j} - \tilde{q}_k\| + \|q_{k+j} - q_k\| \le r_1 \tag{27}$$

where $r_1 = g_1\ d_k + g_2$ with $g_0 = [(1+\gamma_2)^{2K} - 1]$, $g_1 = 2g_0 + 4K\gamma_1\bar{e}$, and $g_2 = 2KTU[1 + \gamma\,\bar{e}(\bar{e} + 2KTU)] + 2g_0\bar{e}$. On the other hand, it is clear that

$$d_k - 2KTU - \bar{e} \le \hat{d}_{k+j} \le d_k + 2KTU + \bar{e}. \tag{28}$$

Moreover, there exist j_1 and j_2 such that

$$\|\tilde{u}_{k+j}\| \ge \mu(d_k - 2KTU - \bar{e}) - r_1 \triangleq r_2, \quad j = j_1, j_2 \tag{29}$$

and we have $\|\phi_{k+j_1}\| = \|\phi_{k+j_2}\| = TU$ if $r_2 \ge U/\beta$. It remains to show that the angle spanned by ϕ_{k+j_1} and ϕ_{k+j_2} lies inside $(\varepsilon^*, \pi - \varepsilon^*)$ with $\varepsilon^* > 0$, which can be achieved by some elementary geometry if $r_2 \ge r_1/2$ is satisfied. Combining with (29), we obtain the excitation of ϕ_t over $[k, k+2K-1]$ if

$$d_k \ge \frac{\max\{g_2/2, U/\beta\} + g_2 + \mu(2KTU + \bar{e})}{\mu - 3g_1/2} \triangleq \bar{d}. \tag{30}$$

3) Stability Analysis: Denote $\Phi_t = I - \gamma\,\phi_t\phi_t'$ and $\Phi_{t_2:t_1} = \Phi_{t_2}\Phi_{t_2-1}\cdots\Phi_{t_1}$. Then, by (24) and (25), it can be found that

$$\begin{aligned}\|\tilde{q}_{k+2K}\| &\le \|\Phi_{k+2K-1:k}\|\|\tilde{q}_k\| + 4K\gamma_1\bar{e}d_k + g_3 \\ &\le (1 - \gamma\,c_0/2)\|\tilde{q}_k\| + 4KTU\gamma\,\bar{e}d_k + g_3\end{aligned} \tag{31}$$

where $g_3 = 2KTU\gamma\,\bar{e}(\bar{e} + 2KTU)$, and the second inequality follows from the excitation of ϕ_t and sufficiently small γ. Furthermore, it follows from (26) that:

$$\begin{aligned}d_{k+2K} \le [(1 - T(\beta-\alpha)s_k) + 4KT^2U\beta\gamma\,\bar{e}]d_k \\ + T\beta\|\tilde{q}_k\| + g_4\end{aligned} \tag{32}$$

where $s_k \ge U/[(\beta+\alpha)(d_k + \bar{e})]$ and $g_4 = T^2U\beta\gamma\,\bar{e}(\bar{e} + 2KTU) + 2KT\alpha\bar{e}$. If γ, β, and $\bar{e}$ are sufficiently small, then $\eta = \min\{\gamma\,c_0/2 - T\beta, T(\beta-\alpha)s_k - 4KTU\gamma\,\bar{e}(1+T\beta)\} > 0$. If we denote $V_k = \|\tilde{q}_k\| + d_k$, then it yields from (31) and (32) that

$$V_{k+2K} \le (1 - \eta)V_k + g_3 + g_4. \tag{33}$$

Therefore, we know that d_k will be ultimately bounded, and hence there exists $s^* > 0$ such that $s_k \ge s^*$ for all k.

4) Ultimate Bound: Recall that $\beta = \nu\gamma$ and $\alpha = \mu\nu\gamma$. We can find small γ so that $d_0 \le \bar{d} < (1+\varepsilon)U/\alpha$ with ε being a small number. Moreover, we have $V_{k+2K} < V_k$ in (33) if $V_k < (g_3 + g_4)/\eta = V^*$. Given $\nu < c_0/(2T)$ and small $\bar{e}$, we can see that $g_3 + g_4 = O(\gamma)$ and $\eta = O(\gamma)$, and hence V^* is smaller than a constant independent of γ. Therefore, if $\bar{d} < d_{k_0} \le (1+\varepsilon)U/\alpha$ with $k_0 = 2n_0K$, then $V_{k_0+2K} < V_{k_0} \le 3d_{k_0}$, and we conclude that $d_k \le 3(1+\varepsilon)U/\alpha \le 4U/\alpha$ for small γ and $k \ge k_0$. Consequently, we find that $s_k \ge \mu U/[3(1+\varepsilon)(1+\mu)U + \alpha(\mu+1)\bar{e}]$, and $T(\beta-\alpha)s_k > 4KTU\gamma\,\bar{e}(1+T\beta)$ follows from (23) and small γ. ■

B. Relative Docking

As introduced earlier, in most real-world applications such as autonomous landing, search, and rescue, it is sufficient to control the UAV to reach a proximity and then rely on visual tracking method to directly estimate the relative position. Hence, the docking objective can be revised to reaching a neighborhood around a location that does not necessarily coincide with the landmark's position; or in other words, given a landmark arbitrarily deployed at an unknown position p^* and

a desired location q^* relative to this landmark, design a control law to achieve

$$\limsup_{k\to\infty} \| p_k - p^* - q^* \| \le \bar{\alpha} \tag{34}$$

where $\bar{\alpha} > 0$ is a user-defined constant.

To solve the above-mentioned problem, we will use the same estimator (7) and modify the controller (8) as follows:

$$\bar{u}_k = \pi_U(u_k), \quad u_k = -\beta(\hat{q}_k - q^*) + \alpha\sigma_k, \ \beta > 0. \tag{35}$$

Due to the similarity in (8) and (35), one would expect that similar results on stability and convergence can be obtained. Indeed, if we define a new relative position state $\bar{q}_k \triangleq p_k - p^* - q^* = q_k - q^*$, we can immediately proceed with the following results on stability and convergence of the system.

Proposition 11: Under the estimator (7) and the bounded controller (35), let condition (12) and Assumption 3 hold. Given the initial values $\tilde{q}_0$ and $\bar{q}_0$, there exists a constant $\bar{M}(\tilde{q}_0)$ to satisfy the following statements.

1) If $\bar{q}_{k_0} \in \bar{\mathcal{M}} \triangleq \bar{\mathcal{B}}(0, \bar{M}(\tilde{q}_0))$ for some k_0, then $\bar{q}_k \in \bar{\mathcal{M}}$ for $k \ge k_0$.
2) There exists a time step $k_0(\bar{q}_0, \bar{\mathcal{M}})$ such that $q_{k_0} \in \bar{\mathcal{M}}$.

Consequently, $\limsup_{k\to\infty} \|\bar{q}_k\| \le \bar{M}(\tilde{q}_0)$ for any $\bar{q}_0$.

Proof: Similar to the proof of Proposition 7, we define $\bar{D}_k = \|\bar{q}\|^2$ and $\Delta\bar{D}_{k+1} = \bar{D}_{k+1} - \bar{D}_k$ and obtain

$$\begin{aligned}\Delta\bar{D}_{k+1}/(sT) \le &-\beta(2 - T\beta)\|\bar{q}\|^2 + 2(1 - T\beta) \\ &\times (\alpha + \beta\|\tilde{q}\|)\|\bar{q}\| + 2\alpha T\beta\|\tilde{q}\| + T\beta^2\|\tilde{q}\|^2 + T\alpha^2. \end{aligned}\tag{36}$$

Note that the leading coefficient of the quadratic function in (36) is negative due to the assumption $T\beta < 1$, hence the boundedness of $\|\bar{q}_k\|$ can be established using the same argument in the proof of Proposition (7). ■

Theorem 12: Under Assumption 3, the relative docking problem (34) can be solved by combining the adaptive estimator (7) and the bounded controller (35), if we select proper gains to satisfy conditions (12). Moreover, the ultimate bound $\bar{\alpha}$ satisfies $\bar{\alpha} \le \alpha/\beta$.

Proof: Based on Proposition 11, we can proceed similarly as in the proof of Theorem 8 to invoke LaSalle's invariance principle and examine the trajectories of $\tilde{q}_k, \bar{q}_k$ in the invariant set defined by $\Delta V_k \equiv 0$. Along the same line as in the proof of Theorem 8, we find that $\tilde{q}_k \equiv 0$. Thus, the dynamics of $\bar{q}_k$ can be simplified as $\bar{q}_{k+1} = \bar{q}_k + T\pi_U[-\beta\bar{q}_k + \alpha\sigma_k]$. By examining $L_k = \|\bar{q}_k\|^2$ and $\Delta L_{k+1} = L_{k+1} - L_k$, we find that $\Delta L_{k+1} < 0$ for $\|\bar{q}_k\| > \alpha/\beta$. On the other hand, if $\|\bar{q}_k\| \le \alpha/\beta$, we have $\|\bar{q}_{k+1}\| = \|(1 - T\beta s_k)\bar{q}_k + Ts_k\alpha\sigma_k\| \le (1 - T\beta s_k)\|\bar{q}_k\| + Ts_k\alpha \le \alpha/\beta$. Therefore, the limit set of those trajectories starting from the invariant set is included in $\bar{\mathcal{B}}(0, \alpha/\beta)$. ■

VI. Simulation

In this section, we will first verify the integrated localization–navigation scheme proposed in Sections III by numerical simulation for an ideal case to verify the theoretical findings. After that, we present another simulation where all possible corruptions of measurements and target drift are added. Finally, another simulation on relative docking will also be presented to verify the results in Theorem 12. Readers interested in studying the effect of changing the gains α, β, γ as well as the influence of different levels of noise to docking and relative docking cases can find the Matlab scripts for all of these simulations at https://github.com/britsknguyen/docking.

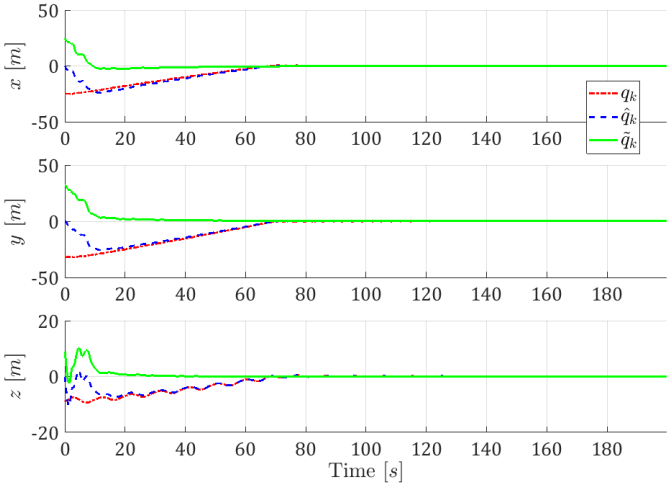

Fig. 1. All trajectories converge to 0 as the gains γ, β, and α satisfy (12).

To be consistent with the experiment setup, we choose $T = 0.1$ s and $U = 0.75$ m/s throughout our simulations. The signal σ_k is generated by (10) and (11) with $\rho_0 = [1, 0]'$, $r_1 = 1/2$, $r_2 = \sqrt{3}/2$, and $N = 96$. For each simulation, we always fix the initial estimate of the relative position as $\hat{q}_0 = [0,\ 0,\ 0]'$, and the initial position of the UAV as $p_0 = [-30,\ -30, 1]'$.

A. Error-Free Case

In this case, we are concerned with a static landmark at $p^* = [-5,\ 2, 10]'$, which yields an initial relative position of $q_0 = [-25,\ 32,\ -9]'$. Under the above setting, we select positive constants $\gamma = 10$, $\beta = 5$, and $\alpha = 4$, which satisfy condition (12). It can be seen in Fig. 1 that all trajectories converge to zero, which validates our theoretical analysis.

B. Corrupted Measurements and Target Drift

Certainly, in practice, we cannot avoid measurement error. To investigate the robustness of the algorithm against measurement errors, we rerun the previous simulation with the presence of all possible errors. First, we add a zero-mean random noise with uniform distribution on the interval $[-0.1, 0.1]$. Second, we also add zero-mean noise with uniform distribution on the interval $[-0.01, 0.01]$ to each of the dimension of displacement measurement. Finally, the landmark is made to drift with its trajectory given as

$$p_k^* = p_0^* + \begin{bmatrix} 5\cos(k\omega) \\ 5\sin(k\omega) \\ 1.25\cos(3k\omega) \end{bmatrix} + kT \begin{bmatrix} -0.05 \\ 0.05 \\ 0.025 \end{bmatrix} \tag{37}$$

where $\omega = 1.534\times10^{-3}$ and $p_0^* = [-5,\ 2,\ 10]$. It can be seen from Fig. 2 that the system is still stable and the UAV can still track the target similar to the ideal case, which demonstrates the robustness of the algorithm in the presence of noise and uncertainty (a drifting landmark).

C. Relative Docking

Different from the docking scenario, in relative docking scenario, α can be chosen arbitrarily according to the desired bound for the docking error α^*. Thus, in this case, we change

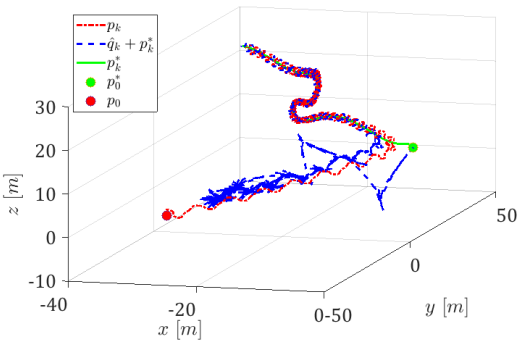

Fig. 2. 3-D visualization of the docking task with all possible corruptions against the ideal scenario. The initial position of the target is marked by the green circle and the UAV's initial position is marked by the red circle.

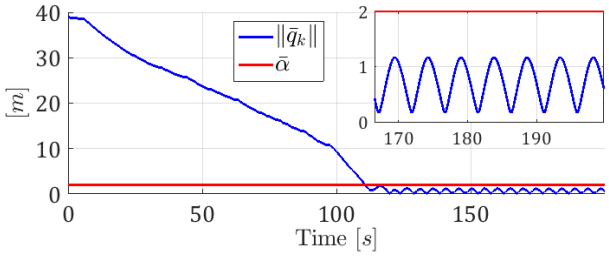

Fig. 3. Relative docking error reduces to below $\bar{\alpha}^* = 2$ m.

for $\alpha = 10$ and the maximum relative docking error $\bar{\alpha}^*$ can be calculated as 2 m, the relative docking position q^* is chosen as $q^* = [-20, 5, 2]'$. All other parameters are the same as the docking case. It can be seen clearly in Fig. 3 that the docking error reduces to below the threshold $\bar{\alpha}$ given by Theorem 12.

VII. Experiments on Quadcopters

To further validate our theoretical findings in Sections IV and V, in this section, we implement the integrated localization–navigation scheme on quadcopters and conduct multiple tests in a GPS-less environment with the docking control law.

For practical purpose, we introduce an additional parameter *terminal distance* d_ϵ, which is to prevent UAV from colliding with the landmark after successfully entering a predefined proximity around the target. In the experiment, we take the terminal distance as 2 m, i.e., $d_\epsilon = 2$. The other parameters are the same as the ones used in the first simulation.

A. Experiment Setup

The algorithm is implemented in real-time on an on-board computer running Ubuntu and robot operating system (ROS). In our experiments, distance measurements d_k are obtained by using two UWB nodes, considering that UWB is robust to multipath and non-line-of-sight effects and can provide a reliable long distance ranging over 100 m with an accuracy within 10 cm (as reported by the sensor's manufacturer[1]). On the other hand, odometry measurements ϕ_k are obtained by fusing the output from *px4flow* optical flow sensor [2] with the measurements from an on-board altimeter and inertial measurement unit using an extended Kalman filter developed and reported in our previous work [5].

[1]https://timedomain.com/products/pulson-440/
[2]https://docs.px4.io/en/sensor/px4flow.html

Fig. 4. Experiment setup.

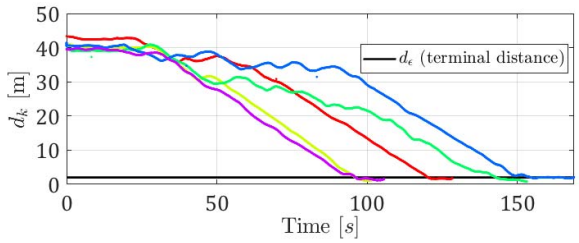

Fig. 5. In all tests, the distance to TUAV is reduced to the terminal value.

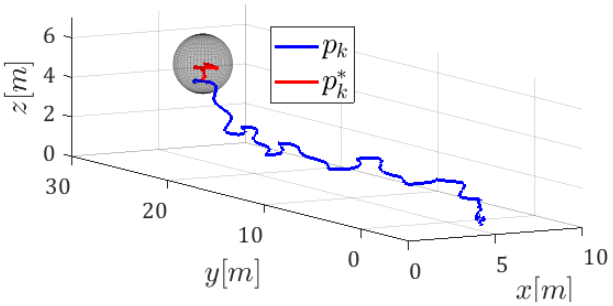

Fig. 6. Spatial trajectory of AUAV as measured by the anchor-based localization system. A ball of radius 2 m is cast around the last recorded position of TUAV to indicate when the AUAV reaches the target.

The flight tests were conducted in a 10 m × 50 m runway surrounded by building blocks. As shown in Fig. 4, one UWB node is mounted on a target UAV (TUAV) stably hovering at some unknown position, and the other one installed on an autonomous UAV (AUAV). The AUAV is required to approach the TUAV from a distant starting point by only using distance measurements and odometry measurements. To provide ground truth for the experiment in the absence of GPS, we employ the anchor-based localization system developed in our previous works [3], which is able to produce 10-cm localization accuracy. It should be emphasized that this localization information is only used as ground truth reference.

B. Experiment Results and Evaluation

A total of five tests with different starting points have been conducted to demonstrate the capability of the integrated localization–navigation scheme (video recording of one test can be watched at https://youtu.be/LJ8mtFIkliY). As shown in Fig. 5, in all cases, the distance between the UAVs decreases steadily and quickly until reaching the terminal distance. To further examine the performance of the estimator and the controller, we select one of the flights and plot its spatial trajectory and time evolution of the system states, respectively, in Fig. 6. It can be seen that AUAV is able to approach TUAV

without much oscillation, if we note that AUAV only moves within [5, 10] on the x-axis during the whole journey, although starting at around 40 m away from TUAV.

In conclusion, the experimental results have shown a good and consistent performance of the proposed integrated localization–navigation scheme, and it is promising to further apply a similar integration idea to more practical scenarios.

VIII. Conclusion

In this brief, we studied the distance-based docking problem of UAVs by using a single landmark placed at an arbitrarily unknown position. An integrated estimation-control scheme by only using distance and odometry measurements was proposed and proved to simultaneously accomplish the relative localization and navigation tasks for discrete-time integrators under bounded velocity. Simulations under different settings were conducted to show the performance and robustness of the algorithm, and the theoretical findings were also validated in a GPS-less environment by implementing the integrated scheme on quadcopters equipped with UWB and optical flow sensors.

References

[1] T.-M. Nguyen, Z. Qiu, M. Cao, T. H. Nguyen, and L. Xie, "An integrated localization-navigation scheme for distance-based docking of UAVs," in *Proc. IEEE/RSJ Int. Conf. Intell. Robots Syst. (IROS)*, Oct. 2018, pp. 5245–5250.

[2] K. Guo *et al.*, "Ultra-wideband-based localization for quadcopter navigation," *Unmanned Syst.*, vol. 4, no. 1, pp. 23–34, 2016.

[3] T. M. Nguyen, A. H. Zaini, K. Guo, and L. Xie, "An ultra-wideband-based multi-UAV localization system in GPS-denied environments," in *Proc. Int. Micro Air Vehicles Conf.*, 2016, pp. 1–6.

[4] C. Wang, H. Zhang, T.-M. Nguyen, and L. Xie, "Ultra-wideband aided fast localization and mapping system," in *Proc. IEEE/RSJ Int. Conf. Intell. Robots Syst. (IROS)*, Sep. 2017, pp. 1602–1609.

[5] T.-M. Nguyen, A. H. Zaini, C. Wang, K. Guo, and L. Xie, "Robust target-relative localization with ultra-wideband ranging and communication," in *Proc. IEEE Int. Conf. Robot. Automat. (ICRA)*, May 2018, pp. 2312–2319.

[6] H. Zou, L. Xie, Q.-S. Jia, and H. Wang, "Platform and algorithm development for a rfid-based indoor positioning system," *Unmanned Syst.*, vol. 2, no. 3, pp. 279–291, 2014.

[7] R. Olfati-Saber, "Flocking for multi-agent dynamic systems: Algorithms and theory," *IEEE Trans. Autom. Control*, vol. 51, no. 3, pp. 401–420, Mar. 2006.

[8] M. Deghat, B. D. O. Anderson, and Z. Lin, "Combined flocking and distance-based shape control of multi-agent formations," *IEEE Trans. Autom. Control*, vol. 61, no. 7, pp. 1824–1837, Jul. 2016.

[9] X. Dong, B. Yu, Z. Shi, and Y. Zhong, "Time-varying formation control for unmanned aerial vehicles: Theories and applications," *IEEE Trans. Control Syst. Technol.*, vol. 23, no. 1, pp. 340–348, Jan. 2015.

[10] K. Z. Y. Ang *et al.*, "High-precision multi-UAV teaming for the first outdoor night show in Singapore," *Unmanned Syst.*, vol. 6, no. 1, pp. 39–65, 2018.

[11] T.-M. Nguyen, X. Li, and L. Xie, "Barrier coverage by heterogeneous sensor network with input saturation," in *Proc. 11th Asian Control Conf. (ASCC)*, Dec. 2017, pp. 1719–1724.

[12] B. Zhu, A. H. B. Zaini, and L. Xie, "Distributed guidance for interception by using multiple rotary-wing unmanned aerial vehicles," *IEEE Trans. Ind. Electron.*, vol. 64, no. 7, pp. 5648–5656, Jul. 2017.

[13] S. Shen, N. Michael, and V. Kumar, "Autonomous multi-floor indoor navigation with a computationally constrained MAV," in *Proc. IEEE Int. Conf. Robot. Automat.*, May 2011, pp. 20–25.

[14] G. Loianno, C. Brunner, G. McGrath, and V. Kumar, "Estimation, control, and planning for aggressive flight with a small quadrotor with a single camera and IMU," *IEEE Robot. Autom. Lett.*, vol. 2, no. 2, pp. 404–411, Apr. 2017.

[15] H. Teimoori and A. V. Savkin, "Equiangular navigation and guidance of a wheeled mobile robot based on range-only measurements," *Robot. Auton. Syst.*, vol. 58, no. 2, pp. 203–215, 2010.

[16] A. S. Matveev, H. Teimoori, and A. V. Savkin, "Range-only measurements based target following for wheeled mobile robots," *Automatica*, vol. 47, no. 1, pp. 177–184, 2011.

[17] Y. Cao, "UAV circumnavigating an unknown target under a GPS-denied environment with range-only measurements," *Automatica*, vol. 55, pp. 150–158, May 2015.

[18] G. Chaudhary, A. Sinha, T. Tripathy, and A. Borkar, "Conditions for target tracking with range-only information," *Robot. Auton. Syst.*, vol. 75, pp. 176–186, Jan. 2016.

[19] I. Shames, S. Dasgupta, B. Fidan, and B. D. O. Anderson, "Circumnavigation using distance measurements under slow drift," *IEEE Trans. Autom. Control*, vol. 57, no. 4, pp. 889–903, Apr. 2012.

[20] B. Fidan, S. Dasgupta, and B. D. O. Anderson, "Adaptive range-measurement-based target pursuit," *Int. J. Adapt. Control Signal Process.*, vol. 27, nos. 1–2, pp. 66–81, Jan./Feb. 2013.

[21] S. Güler, B. Fidan, S. Dasgupta, B. D. O. Anderson, and I. Shames, "Adaptive source localization based station keeping of autonomous vehicles," *IEEE Trans. Autom. Control*, vol. 62, no. 7, pp. 3122–3135, Jul. 2017.

[22] S. H. Dandach, B. Fidan, S. Dasgupta, and B. D. O. Anderson, "A continuous time linear adaptive source localization algorithm, robust to persistent drift," *Syst. Control Lett.*, vol. 58, no. 1, pp. 7–16, 2009.

[23] G. Chai, C. Lin, Z. Lin, and M. Fu, "Single landmark based collaborative multi-agent localization with time-varying range measurements and information sharing," *Syst. Control Lett.*, vol. 87, pp. 56–63, 2016.

[24] G. Chai, C. Lin, Z. Lin, and W. Zhang, "Consensus-based cooperative source localization of multi-agent systems with sampled range measurements," *Unmanned Syst.*, vol. 2, no. 3, pp. 231–241, 2014.

[25] B. Fidan, A. Çamlıca, and S. Güler, "Least-squares-based adaptive target localization by mobile distance measurement sensors," *Int. J. Adapt. Control Signal Process.*, vol. 29, no. 2, pp. 259–271, Feb. 2015.

[26] P. Iannou and B. Fidan, *Adaptive Control Tutorial*. Philadelphia, PA, USA: SIAM, 2006.

[27] W. Mei and F. Bullo. (2017). "Lasalle invariance principle for discrete-time dynamical systems: A concise and self-contained tutorial." [Online]. Available: https://arxiv.org/abs/1710.03710